

taken place. The second state, a conformational intermediate that accumulates before cleavage under active conditions in the crystal, was captured by freeze-trapping the RNA 4 min after Mg^{2+} was added at pH 8.5 to induce cleavage.

Hammerhead RNA self-cleavage requires one or more catalytic divalent metal ions, one of which ionizes the 2'-hydroxyl at the cleavage site. The newly generated nucleophile attacks the adjacent phosphate by an in-line mechanism. The same metal ion, or perhaps another, stabilizes the pentacoordinated phosphate transition state by binding directly to the pro-R phosphate oxygen. The reaction generates 5'-hydroxyl and 2',3'-cyclic phosphate termini at the cleavage site (7).

In solution, the rate of hammerhead ribozyme cleavage increases with pH (8). The uncleaved, unmodified hammerhead RNA enzyme and substrate strands were prepared as reported (9), and crystallized in 1.8 M Li_2SO_4 , 1.25 mM EDTA, and 50 mM sodium cacodylate buffered at pH 6.0. The RNA used for crystallization was completely cleaved in solution in less than 5 min in the crystallization conditions augmented with Mg^{2+} ions. However, in the crystal, the hammerhead RNA was not cleaved after 30 min at pH 7.0 in the presence of 100 mM $MgSO_4$, but does cleave (90 percent within 15 min) at pH 8.5 (Fig. 2). Our data show that hammerhead RNA can cleave itself in the crystalline state (although more slowly and under more basic conditions

than required in solution), an indication that the RNA fold found in the crystal structure is that of a biologically active hammerhead RNA. This conclusion is corroborated by earlier published studies (10). Cleavage of the RNA in solution is an entropy-driven process, due to cleavage product release (11). Lattice contacts prevent product release in the crystal, slowing the cleavage rate.

We solved the crystal structure of the uncleaved, unmodified hammerhead RNA by molecular replacement; and used the previously solved (3) 2'-modified hammerhead RNA structure as a probe. The two other crystal structures that we solved were obtained in the presence of divalent metal ions, one at pH 5 and the other at pH 8.5. Each crystal was stabilized in a cryoprotectant composed of 20% glycerol, 1.8 M Li_2SO_4 buffered at the appropriate pH (either in the presence or absence of divalent metal ions), and then flash-frozen in liquid propane and maintained at 100 K (Table 1).

We used Mn(II) to obtain the metal-bound structure cleavage-arrested at pH 5, allowing us to use its anomalous scattering properties to identify the divalent metal ion binding sites. Because $MnSO_4$ slowly forms insoluble oxides at pH 8.5, we used 100 mM $MgSO_4$ for the cleavage experiments at higher pH. Although stable at lower pH, the hammerhead RNA crystals deteriorate within 5 min at pH 8.5 in the presence of $MgSO_4$ as the RNA is cleaved. We therefore flash-froze the crystals for data collection after 4 min of exposure to the pH 8.5 cleavage solution. The freeze-trapped intermediate experiment was repeated with Mn(II) to confirm the assigned Mg(II) sites.

The unmodified hammerhead RNA crystal structures thus solved, obtained in the absence of divalent metal ions at pH 6.0 and in their presence at pH 5.0, are similar to the modified hammerhead ribozymes. The freeze-trapped intermediate structure, however, revealed a significant conformational change. As with the modified ribozyme structures, the lower pH structures both reveal that the scissile phosphodiester bond and the adjacent ribose are still in approximate A-form helical conformation. As a result, these structures all place the 2'-nucleophile site approximately 3.5 Å from the phosphate atom, but on the wrong side of the group for an S_N2 displacement to occur. Because the modified structures were not in a conformation that would support in-line strand cleavage (2, 3), it had been proposed that the absence of an unmodified 2'-hydroxyl at the cleavage site in each case might have corrupted the structures, and that a significant conformational change must occur before or during cleavage (5). However, our unmodified RNA crystal

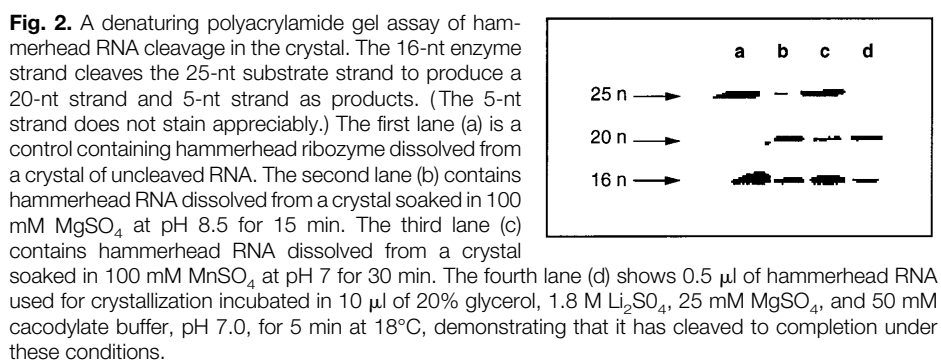


Table 1. Data collection statistics. Native unmodified ribozyme crystals and Mn(II)-soaked ribozyme crystals at lower pH were analyzed at Brookhaven National Laboratory synchrotron beamline X12C with 1.4 Å x-rays and a 30-cm MAR imaging plate detector on crystals flash-frozen in the reservoir solution containing 20% glycerol as a cryoprotectant. Data on the crystals at higher pH with Mg(II) soaked in were collected at Daresbury Laboratory synchrotron beamline PX7.2 with 1.488 Å x-rays under otherwise similar conditions. (This experiment was repeated at X12C with Mn(II), confirming the results of the Mg(II) experiments.) The crystals were flash-frozen in liquid propane cooled by liquid nitrogen, and then transferred to a 100K cold stream (Oxford Cryosystems). The images were processed with DENZO and SCALEPACK (17) and standard crystallographic computations were performed within CCP4 (18). The space group was $P3_121$.

Item	Native pH 6.0	Mn(II) pH 5.0	Mg(II) pH 8.5
	<i>Data collection</i>		
Synchrotron x-ray source	X12C*	X12C*	PX7.2†
Wavelength (Å)	1.400	1.400	1.488
Resolution range (Å)	43.0–3.0	43.0–3.0	22.8–3.1
Unique reflections (<i>N</i>)	7003	6716	6561
Redundancy of data	3.4	7.7	6.7
<i>I</i> / σ (<i>I</i>)	15.9	13.5	12.5
Reciprocal space coverage (%)	97.3	93.6	99.1
Resolution (<i>N</i>)			
Completeness (<i>F</i> > 2 σ)(%)	85.4	83.3	92.2
<i>R</i> _{scale} (all data) (%)	6.8	7.2	11.5
Mosaicity (°)	0.5	0.6	1.0
Cell (<i>a</i> , <i>c</i>) for $P3_121$ (Å)	64.56, 136.29	64.55, 135.87	65.90, 136.77
Isomorphous differences (%)	0	16.6	25.9
Divalent metal ions assigned		5	5
	<i>Refinement</i>		
<i>R</i> factor (<i>F</i> > 2 σ) (%)	21.6	21.7	24.7
<i>R</i> _{free} (10% of data) (%)	26.5	26.2	29.7
Bond lengths (Å) rmsd	0.007	0.010	0.010
Bond angles (°) rmsd	1.1	1.4	1.5
Torsion angles (°) rmsd	13.0	16.5	16.8
Planar angles (°) rmsd	1.5	1.6	1.7

*Brookhaven National Laboratory NSLS. †Daresbury Laboratory SLS.

structures all have intact 2'-hydroxyls at the cleavage site, and the relevant phosphate backbone conformation remains unchanged when compared to the two modified hammerhead RNA structures, demonstrating that this is in fact the natural conformation of the catalytically active ground-state hammerhead RNA.

In contrast, the freeze-trapped pH 8.5 structure (Fig. 3A) reveals a significant conformational change in the region of the cleavage site, induced by the cleavage reaction conditions, whereas the rest of the molecule remains essentially unchanged. The conformational change is most pronounced in the substrate strand cleavage-site nucleotide (C17) phosphodiester backbone and base, as well as in the backbone of the residue immediately 3' to the cleavage site (A1.1) (Fig. 1). This results in a localized upward translation of the substrate strand relative to the catalytic pocket. (Fig. 3B). The relevance of the location of this conformational change is immediately apparent, as it is the scissile phosphodiester bond, located between C17 and A1.1, which moves the most (2.9 Å). The averaged movement of the ribose and phosphate between C17 and A1.1 is 2.0 Å, and of the ribose and phosphate 5' to C17 is 1.8 Å. (The corresponding differences between the unmodified hammerhead RNA in the absence of metal ions and the 2'-methoxyl-substituted RNA determined from a different crystal form are 0.535 Å for C17 and 0.532 Å for A1.1; Fig. 3B.)

In addition to the backbone conformational change in the substrate strand, the

base and sugar of C17 move relative to the catalytic pocket residues. C17 is no longer within good hydrogen bonding distance of C3, moving from 3.2 to 3.65 Å apart. In addition, the furanose oxygen (O_4') of the ribose of C17 no longer interacts directly with the base of A6 in the catalytic pocket, but rather the nucleotide as a whole has pivoted outward such that a fairly good base-stacking interaction between C17 and A6 is achieved. In turn, G5 and A6 pivot slightly upward either to accommodate C17 in this changed conformation or perhaps to induce it (Fig. 4A.)

The freeze-trapped conformational intermediate is stabilized primarily by a new hydrogen bond that forms between the furanose oxygen of C17 and the 2'-hydroxyl of U16.1 (Fig. 4A, white dotted line). In addition, the hydrogen bonding distance between the endocyclic nitrogen N3 of A6 and the 2'-hydroxyl of U16.1 is now decreased from 3.1 to 2.6 Å. These hydrogen bonds perhaps compensate for the loss of the hydrogen bond between C17 and C3 caused by the conformational change. Both hydrogen bond interactions are consistent with the observation that replacing U16.1 with deoxythymine significantly reduces the activity of the hammerhead RNA (12). It is quite possible that this elimination of the potential for hydrogen bond formation between the 2'-hydroxyl of U16.1 and the furanose oxygen of C17 would destabilize the structure of the conformational intermediate, thus accounting for the observed diminished (22 times lower) activity in such a ribozyme.

All of the Mn(II) sites identified in the lower pH structure [several of which were observed previously (2, 3)] reappear as Mg(II) sites in the freeze-trapped intermediate structure (Fig. 3A). An additional Mg(II) bound directly to the pro-R phosphate oxygen adjacent to the scissile bond appears prominently in the crystal structure of the pH 8.5 intermediate (Fig. 4A, site 6). This Mg(II) ion, when unconstrained during refinement, appears to be 2.2 to 2.4 Å from the pro-R phosphate oxygen (the optimal distance in a constrained refinement would be 2.1 Å). This geometry is compatible with a metal ion bound directly to the oxygen atom (as it is too close to be a water molecule). It fulfills the condition for being the Mg(II) site previously inferred on the basis of biochemical evidence as critical to the catalytic activity of the hammerhead ribozyme (13), and its authenticity [as well as that of the other Mg(II) sites] was substantiated by repetition of this experiment with Mn(II). The additional metal ion site (Figs. 3B and 4A, site 6), found only in the conformational intermediate structure, is more relevant to the cleavage mechanism than is the previously identified site 3 Mg(II). Its implications are discussed below.

An additional metal ion site appearing in both of the metal-bound structures near G5 in the catalytic pocket (Figs. 3B and 4A, site 4) is of interest because of the rigorous requirement for all the functional groups of G5; alteration of any of these affects ribozyme cleavage (5). In addition, G5 has been implicated in binding a uranium ion, as evidenced by uranium-induced cleavage at

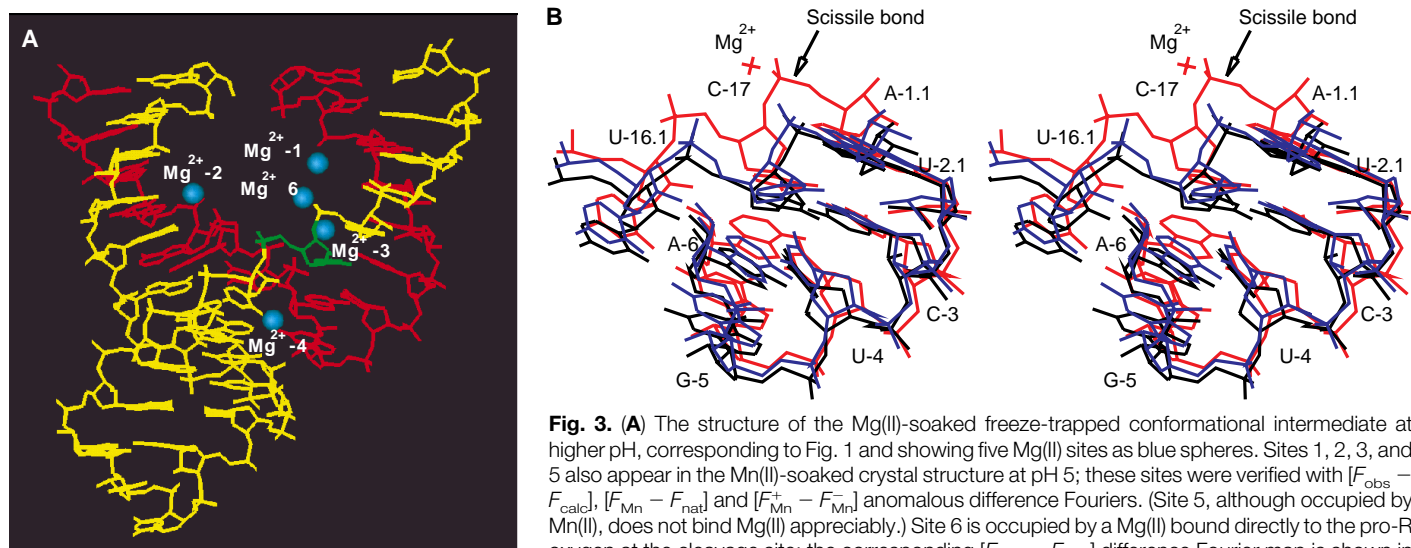


Fig. 3. (A) The structure of the Mg(II)-soaked freeze-trapped conformational intermediate at higher pH, corresponding to Fig. 1 and showing five Mg(II) sites as blue spheres. Sites 1, 2, 3, and 5 also appear in the Mn(II)-soaked crystal structure at pH 5; these sites were verified with $[F_{\text{obs}} - F_{\text{calc}}]$, $[F_{\text{Mn}} - F_{\text{nat}}]$ and $[F_{\text{Mn}}^+ - F_{\text{Mn}}^-]$ anomalous difference Fouriers. (Site 5, although occupied by Mn(II), does not bind Mg(II) appreciably.) Site 6 is occupied by a Mg(II) bound directly to the pro-R oxygen at the cleavage site; the corresponding $[F_{\text{obs}} - F_{\text{calc}}]$ difference Fourier map is shown in

the close-up view of the catalytic pocket in Fig. 4A. Assignment of these peaks as Mg(II) was corroborated by repetition of the experiment in the presence of Mn(II). (B) Stereo diagram of the superposition of the freeze-trapped conformational intermediate, shown in red (with the Mg²⁺ bound to the pro-R phosphate oxygen adjacent to the scissile bond) on both the "ground-state" structure in the same crystal form (before metal ions are introduced) shown in blue, and the 2'-O-methyl C17 modified hammerhead RNA, in a different crystal form, shown in black. The average difference in backbone position between the blue and black structures, a result of the combined effects of differences in crystal packing, crystallization conditions, and coordinate error, is about 0.5 Å. Therefore, the movement of the scissile bond in the freeze-trapped conformational intermediate is best characterized as a 2.9 ± 0.5 Å change in position.

that site (14). The role, if any, of metal ions bound to G5 is not, however, apparent from these structures.

Our previous crystallographic analysis (3) and independent biochemical experiment (15) had each identified a metal located at site 3 in Fig. 3B as possibly relevant to the hammerhead RNA cleavage mechanism. We had originally suggested that the mode of binding observed for the metal at site 3 might have been perturbed by the presence of the 2'-O-methyl-C modification at the cleavage site, and that an unmodified, catalytically active RNA might bind that metal ion in a manner more obviously relevant to the catalytic cleavage mechanism (3). However, this does not appear to be the case, as the site 3 metal binds to the unaltered RNA in the same way. Hence, this divalent metal ion must shift in position relative to the active site (or vice versa) to initiate cleavage (as we proposed previously), or this divalent metal ion is simply playing an ancillary structural role rather than being directly involved in catalysis.

It thus appears that an additional Mg(II) ion, at site 6, binds to the pro-R phosphate oxygen at the cleavage site before the RNA in the crystal adopts a conformation compatible with in-line attack. Several possibilities thus emerge for the mechanism of cleavage.

One possibility is that two Mg(II) ions are required for initiating cleavage: one bound to the pro-R phosphate oxygen at site 6, and the other (possibly originating at site 3) in the form of a metal hydroxide that then attacks the cleavage-site 2'-hydroxyl on further RNA conformational change. Another possibility, which we favor in view of its simplicity and explanatory power, is that a single Mg(II) binds to the pro-R phosphate oxygen at site 6, inducing the conformational change required for in-line attack at the cleavage-site 2'-hydroxyl moiety. In this case, the same metal that binds to the pro-R phosphate oxygen also provides the hydroxide that initiates the base-catalyzed step of the cleavage reaction. The phosphate oxygen-metal complex may alter favorably the effective pK_a of the metal hydroxide, thus activating the cleavage reaction.

At least two types of conformational changes compatible with this one-metal mechanism are possible: (i) The cleavage-site base pivots, as observed, in the conformational intermediate, stacking on A6, and subsequently the Mg(II) in complex with the pro-R phosphate oxygen at site 6 swings downward until a hydroxide bound to it can abstract the proton from the 2'-hydroxyl on the cleavage-site base. At this point in the cleavage reaction, the active Mg(II) can be

positioned by its interaction with C3 of the catalytic pocket, as suggested previously (3) and as shown in Fig. 4B. (ii) The base and sugar of C17 can instead swing upward in a direction opposite to the motion observed in the conformational intermediate structure until the 2'-hydroxyl on the cleavage-site base comes within reach of a hydroxide bound to an immobile metal ion. Although the latter possibility has the advantage that the Mg(II) bound to the pro-R phosphate oxygen at site 6 remains immobile, it has the disadvantage that C17 would suffer an energetic penalty for becoming unstacked and for breaking one or more hydrogen bonds.

Possibility (i), in which C17 remains stacked and hydrogen-bonded as observed in the freeze-trapped intermediate structure, has the merit of compatibility with the experimentally observed conformational change in the cleavage-activated intermediate structure and does not require base unstacking or hydrogen bond breakage. Positioning the metal ion-phosphate complex for in-line attack would require only adjustments of the backbone angles β , γ , δ , and ϵ of nucleotide A1.1 (at the cleavage site) (Fig. 4B); β , γ , and δ , as well as the conformation of C17, change minimally and in the same direction to form this transition-state geometry as they do to achieve the observed intermediate conformation relative to the ground-state one. Whatever the details of the path to this transition state, the required atomic movements are small and localized; in particular, the Mg(II) is required to move about 2 Å. Moreover, the direction of movement of the phosphate backbone needed to arrive at the transition state would continue that used to produce the conformational intermediate. Therefore, we favor the mechanism in which the metal ion-phosphate complex rotates relative to the rest of the RNA molecule to reach the proposed transition state (Fig. 4B).

It is possible that the freeze-trapped conformational intermediate we have captured accumulates to near full occupancy in the crystal (thus allowing observation) due to constraints imposed by crystal packing, and would not accumulate appreciably as a transient intermediate in solution. If this is the case, it may be fortuitous that lattice packing has the effect of increasing the depth of the local potential energy minimum corresponding to the conformational intermediate while preserving the overall shape of the potential energy surface of the reaction pathway. This local alteration would allow accumulation of an intermediate in a manner analogous to that deliberately used in a previous Laue time-resolved experiment. In that experiment (16), site-directed mu-

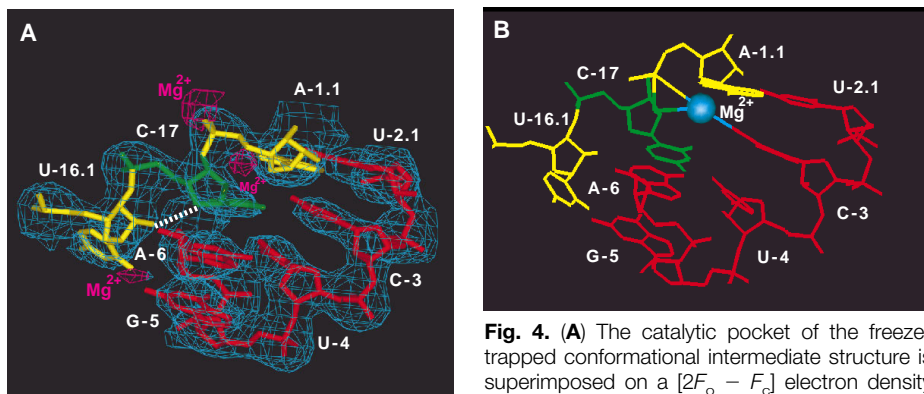


Fig. 4. (A) The catalytic pocket of the freeze-trapped conformational intermediate structure is superimposed on a $[2F_o - F_c]$ electron density map generated with the refined structure of the RNA alone, shown in light blue. (The structure was verified with simulated annealing omit maps with C17 and A1.1 omitted from the refinement.) The new hydrogen bond between the furanose oxygen of C17 and the 2'-hydroxyl of U16.1 is indicated with a white dashed line. In addition, three difference Fourier peaks representing Mg(II) sites are shown in pink, contoured at 3.0σ . Site 6 appears to be a Mg(II) coordinated directly to the pro-R oxygen of the cleavage-site phosphate adjacent to the scissile bond, and is found only in the higher pH intermediate structure. Another peak (site 3) appears to be a fully hydrated Mg(II) which makes through-water contacts to C3 and C17 as observed in our previous structure of the 2'-modified RNA (3). A peak similar to this one appears as Mn(II) in the lower pH structure of the unmodified RNA, but does not appear in the structure where no divalent metal ions have been introduced. Site 4, the weak peak adjacent to G5, appears more strongly in the Mn(II)-soaked crystals. (B) A proposed transition-state structure, postulated on the basis of the intermediate structure (Fig. 3A) as well as on Mg(II) binding to the uridine turn of the tRNA^{Phe} anticodon loop, as discussed (3), contains an Mg(II) bound to the pro-R oxygen adjacent to the scissile bond at site 6. The base of C17 stacks on A6, as suggested by the freeze-trapped intermediate structure. The phosphate backbone between C17 and A1.1, with the Mg(II) attached to the pro-R oxygen, moves from the position in the configurational intermediate (A) toward the 2'-hydroxyl of the ribose to accommodate a geometry compatible with in-line attack. This results in positioning the Mg(II) in such a way that a through-water contact would be made to C3 of the catalytic pocket, as proposed previously (3), and an additional contact with the exocyclic oxygen of C17 would also be possible.

togenesis was used to create two "kinetic bottlenecks" in the reaction pathway of isocitrate dehydrogenase, greatly extending the lifetime of each of two transient intermediates, enabling their observation. In the present context, it is possible that the lattice contacts themselves have created such a kinetic bottleneck, enabling us to freeze-trap a conformational intermediate prior to RNA catalytic cleavage. Kinetic bottleneck mutants of the hammerhead RNA should allow capture of additional cleavage reaction intermediates.

REFERENCES AND NOTES

1. C. Guerrier-Takada, K. Gardiner, T. Marsh, N. Pace, S. Altman, *Cell* **35**, 849 (1983); A. J. Zaug, T. R. Cech, *Science* **231**, 470 (1986).
2. H. W. Pley, K. M. Flaherty, D. B. McKay, *Nature* **372**, 111 (1994).
3. W. G. Scott, J. T. Finch, A. Klug, *Cell* **81**, 991 (1995).
4. O. C. Uhlenbeck, *Nature* **328**, 596 (1987); D. E. Ruffner, G. D. Stormo, O. C. Uhlenbeck, *Biochemistry* **29**, 10695 (1990).
5. D. B. McKay, *RNA* **2**, 395 (1996).
6. K. Moffat and R. Henderson, *Curr. Opin. Struct. Biol.* **5**, 656 (1995).
7. W. Scott and A. Klug, *Trends Biochem. Sci.* **21**, 220 (1996).
8. S. Dahm and O. C. Uhlenbeck, *Biochemistry* **30**, 9464 (1991); S. Dahm, W. Derrick, C. Uhlenbeck, *ibid.* **32**, 13040 (1993).
9. J. B. Murray, A. K. Collier, J. R. P. Arnold, *Anal. Biochem.* **218**, 177 (1994); W. G. Scott et al., *J. Mol. Biol.* **250**, 327 (1995).
10. T. Tushl et al., *Science* **266**, 785 (1994); S. T. Sigurdsson, T. Tushl, F. Eckstein, *RNA* **1**, 575 (1995); K. M. A. Amiri and P. J. Hagerman, *J. Mol. Biol.* **261**, 125 (1996).
11. K. J. Hertel and O. C. Uhlenbeck, *Biochemistry* **34**, 1744 (1995).
12. J.-H. Yang et al., *ibid.* **29**, 11156 (1990).
13. H. van Tol et al., *Nucleic Acids Res.* **18**, 1971 (1990); G. Slim and M. J. Gait, *ibid.* **19**, 1183 (1991); M. Koizumi and E. Ohtsuka, *Biochemistry* **30**, 145 (1991).
14. G. S. Bassi et al., *Nature Struct. Biol.* **2**, 45 (1995).
15. J. B. Murray, C. J. Adams, J. R. P. Arnold, P. G. Stockley, *Biochem. J.* **311**, 487 (1995).
16. J. M. Bolduc et al., *Science* **268**, 1312 (1995).
17. Diffraction data were processed with DENZO [Z. Otwinowski, in *Proceedings of the CCP4 Study Weekend*, L. Sawyer, N. Isaacs, S. Bailey, Eds. [Daresbury, U.K., and SERC, 1993], pp. 56–62]. Further details are described in Table 1.
18. Molecular replacement was done with the AMoRe (automated molecular replacement) software distributed with CCP4 (19) and, as a probe, the dimer structure determined from the previous crystal form. The top translation function solution had an *R* factor of 53% and a correlation coefficient of 28. However, 10 cycles of rigid-body refinement in AMoRe reduced the *R* factor to 31%, and the correlation coefficient simultaneously increased to 86. Further rigid-body refinement followed by conventional positional refinement (Powell minimization) in X-PLOR 3.1 [A. T. Brünger, *X-PLOR 3.1: A System for Crystallography and NMR* (Yale Univ. Press, New Haven, CT, 1993)] further reduced the *R* factor to 26%. The initial model of one hammerhead ribozyme molecule in the crystal asymmetric unit was further refined with a standard simulated annealing slow-cooling molecular dynamics protocol followed by conventional positional and restrained temperature factor refinement in X-PLOR 3.1 with data from 8.0 to 3.0 Å resolution and a modified RNA geometry parameter library [G. Parkinson, J. Vojtechovsky, L. Clowney, A. T. Brünger, H. M. Berman, *Acta Crystallogr.* **D52**, 57 (1996)]. Finally, the low resolution data were incorporated, a solvent mask was determined,

- and partial calculated structure factors were generated to model the bulk solvent contribution to the x-ray scattering amplitudes for further refinement within X-PLOR 3.1. The metal-bound crystal structures were refined identically (Table 1).
19. Collaborative Computational Project, Number 4 [CCP4], *Acta Crystallogr.* **D50**, 760 (1994).
 20. We thank P. Stockley, J. Finch, G. Varani, S. Price, K. Nagai, O. Uhlenbeck, and members of their research groups for advice; R. Sweet for help with data collec-

tion at Brookhaven synchrotron beamline X12C, and the Daresbury Laboratory for additional data collection; D. McKay and K. Flaherty for discussions and for providing us with an improved set of stereochemical parameters (18) for RNA refinement. Supported by the Medical Research Council of the United Kingdom and the American Cancer Society (W.G.S., PF-3970), and the NIH (B.L.S., GM-49857).

21 May 1996; accepted 26 October 1996

Functional Analysis of the Genes of Yeast Chromosome V by Genetic Footprinting

Victoria Smith, Karen N. Chou, Deval Lashkari, David Botstein, Patrick O. Brown*

Genetic footprinting was used to assess the phenotypic effects of Ty1 transposon insertions in 268 predicted genes of chromosome V of *Saccharomyces cerevisiae*. When seven selection protocols were used, Ty1 insertions in more than half the genes tested (157 of 268) were found to result in a detectable reduction in fitness. Results could not be obtained for fewer than 3 percent of the genes tested (7 of 268). Previously known mutant phenotypes were confirmed, and, for about 30 percent of the genes, new mutant phenotypes were identified.

The completion of the sequences of the genomes of several microorganisms is a watershed for the new science of genomics. The next important challenge is to determine, in an efficient and reliable way, something about the function of each gene in these genomes. The 12,057-kb nonrepetitive portion of the *S. cerevisiae* genome—the first completely sequenced eukaryotic genome—contains 6000 to 6500 predicted genes, of which fewer than half had previously been known. A still smaller fraction of the genes of yeast have been characterized experimentally with respect to biological function; indeed, previous work suggested that disruption of yeast genes resulted in a readily discernible phenotype only about 30% of the time (1). Here, we describe the results of genetic footprinting (2) as applied to 268 predicted protein-coding genes on chromosome V of *S. cerevisiae* (3).

We subjected a large population of haploid yeast cells ($\sim 10^{11}$ cells) to mutagenesis by transiently inducing transposition of a marked Ty1 transposable element. DNA was extracted from a portion of this culture (the "time-zero" DNA). Other representa-

tive samples of this population were subjected to one of several selections (Table 1). DNA was extracted from the cells recovered after each selection. The presence and relative abundance of cells carrying Ty1 insertions within a gene of interest was assessed for each of these samples by means of a polymerase chain reaction (PCR) (2). In general, for each gene, we surveyed a minimum of 500 to 900 base pairs (bp) of coding sequence, along with 400 to 600 bp of upstream sequence. Smaller genes (<700 bp) were analyzed in their entirety, along with several hundred base pairs of sequence flanking the start and stop codons. A growth disadvantage to cells carrying insertions in a gene, under a particular selection, was reflected by the loss or depletion of the PCR products representing those insertions (the "genetic footprint") when DNA samples from the selected population were compared with the time-zero DNA samples. The method not only detects severe growth disadvantages, but also sensitively measures moderate reductions in fitness.

For each predicted protein-coding sequence on chromosome V, a color was assigned on the basis of whether a particular selection protocol resulted in a perceptible depletion of the PCR products representing insertions in that coding sequence (Fig. 1). Overall, we were able to obtain satisfactory genetic footprinting data for 261 (97%) of the predicted protein-coding genes (4, 5). This total includes six putative genes contained in repeated telomeric sequences (boxed in Fig. 1): cells with mutations in any of these six genes appeared wild type for

V. Smith and K. N. Chou, Department of Biochemistry, Stanford University School of Medicine, Stanford, CA 94305, USA.

D. Lashkari and D. Botstein, Department of Genetics, Stanford University School of Medicine, Stanford, CA 94305, USA.

P. O. Brown, Howard Hughes Medical Institute and Department of Biochemistry, Stanford University School of Medicine, Stanford, CA 94305, USA.

*To whom correspondence should be addressed. E-mail: pbbrown@cmgm.stanford.edu